

Boundary Phosphate Transport of the East China Sea and Its Influence on Biological Process

Zhijian Lin¹, Xiaochun Wang^{1*}, Peng Xiu², Fei Chai³, Qiong Wu¹

¹School of Marine Sciences, Nanjing University of Information Science and Technology, Nanjing, China

²State Key Laboratory of Tropical Oceanography, South China Sea Institute of Oceanology, Chinese Academy of Sciences, Guangzhou, China

³State Key Laboratory of Satellite Ocean Environment Dynamics, Second Institute of Oceanography, Ministry of Natural Resources, Hangzhou, China
Email: *xcwang@nuist.edu.cn

How to cite this paper: Lin, Z. J., Wang, X. C., Xiu, P., Chai, F., & Wu, Q. (2019). Boundary Phosphate Transport of the East China Sea and Its Influence on Biological Process. *Journal of Geoscience and Environment Protection*, 7, 79-104.
<https://doi.org/10.4236/gep.2019.79007>

Received: April 2, 2019

Accepted: September 21, 2019

Published: September 24, 2019

Copyright © 2019 by author(s) and Scientific Research Publishing Inc. This work is licensed under the Creative Commons Attribution International License (CC BY 4.0).
<http://creativecommons.org/licenses/by/4.0/>



Open Access

Abstract

The East China Sea (ECS) is one of the largest marginal seas in the Northwest Pacific, and also one of the most productive regions of the global ocean. Using a three-dimensional Pacific physical-biological model, we investigate the interannual variation of phosphate transport via Kuroshio intrusion (KIPT) in the eastern boundary of the East China Sea (ECS) and its influence on the ECS biological process during 1997 to 2016. The KIPT into the ECS mainly occurs in the northeast of Taiwan and southwest of Kyushu, with stronger interannual variability in the northeast of Taiwan. The variation of the KIPT is more significant in the near-bottom water, and is dominated by volume transport. On the interannual timescale, the KIPT changes in response to the shift of the Kuroshio axis and to the bottom upwelling in the ECS eastern boundary. When the Kuroshio axis is closer to (farther away from) the ECS shelf, the strength of the bottom upwelling increases (decreases). This process induces more (less) significant topographic beta spiral, which causes an anti-cyclonic (cyclonic) eddy-like bottom velocity feature in the northeast of Taiwan. Eventually, more phosphate is transported to the ECS inner shelf, which increases chlorophyll concentration around the Zhoushan Islands and Yangtze Estuary but reduces chlorophyll concentration in the ECS outer shelf. Conversely, the chlorophyll increases in the ECS outer shelf but decreases around the Zhoushan Islands and Yangtze Estuary when there is less phosphate transport. This study highlights the importance of Kuroshio intrusion in connecting the inner and outer shelves of the ECS on the interannual timescale. Phosphate transport into the East China Sea via Kuroshio intrusion shows

great interannual variability in the northeast of Taiwan. On the interannual timescale, the variation of phosphate transport into the East China Sea via Kuroshio intrusion is dominated by volume transport. When the Kuroshio axis is closer to the East China Sea shelf, there is more phosphate transport into the East China Sea, and chlorophyll increases around the Zhoushan Islands and Yangtze Estuary.

Keywords

Boundary Phosphate Transport, East China Sea, Biological Process

1. Introduction

The East China Sea (ECS) is one of the largest marginal seas in the Northwest Pacific. Over 75% of the ECS is continental shelf (**Figure 1**). The ECS connects with the South China Sea and Japan Sea through the Taiwan Strait and Korea Strait on the south and north, respectively. To the east, the ECS meets the Ryukyu Islands chain and Kyushu Island of Japan, which are along the flow direction of the Kuroshio. To the west, it is bounded by the Asian continent.

The ECS is also one of the most productive regions of the global ocean because of huge amount of externally sourced nutrients (Guo, 1994; Iseki, 1995; Wei et al., 2003), which are mainly from river discharges and Kuroshio intrusion (Wollast, 1991, 1993; Ladd et al., 2005; Whitney et al., 2005; Sugimoto et al., 2009). The river-derived nutrients are mainly from the Yangtze River, which provides a combined annual input of 3.17 kmol/s nitrogen and 0.03 kmol/s phosphorous to the ECS (Chen & Wang, 1999). However, many studies reported that the Kuroshio water supplies several times of nutrients, much more than the rivers (Zhang et al., 1997; Chen & Wang, 1999; Zhang et al., 2007; Isobe & Matsuno, 2008). Based on observed and estimated data, Chen (2008) demonstrated that the nutrients of the Kuroshio water contribute 49% (4.69 kmol/s) of the externally sourced nitrogen and 71% (0.34 kmol/s) of the phosphorous for the ECS. This indicated that the phosphorous from the Kuroshio water might play a more important role in the ECS biological process. Guo et al. (2012) confirmed this because the ratio of phosphate to nitrate concentration (P:N ratio: 1:13.64) in the Kuroshio water is higher than that consumed by phytoplankton as indicated by the Redfield ratio (1:16). Worthwhile pointing out that the P:N ratio (<1:100) in riverine nutrients is far lower than the Redfield ratio, which could lead to phosphorous limitation in the estuary. Wang et al. (2003) also suggested that the ECS primary production is limited by phosphate rather than by nitrate. Thus, the variation of phosphate transport via Kuroshio intrusion (KIPT) into the ECS is a crucial factor that influences the change of the ECS biological process, especially for the area of phosphorous limitation.

The annual-averaged KIPT into the ECS takes place in the northeast of Taiwan and southwest of Kyushu, but there is an outflow along the 200-m isobath

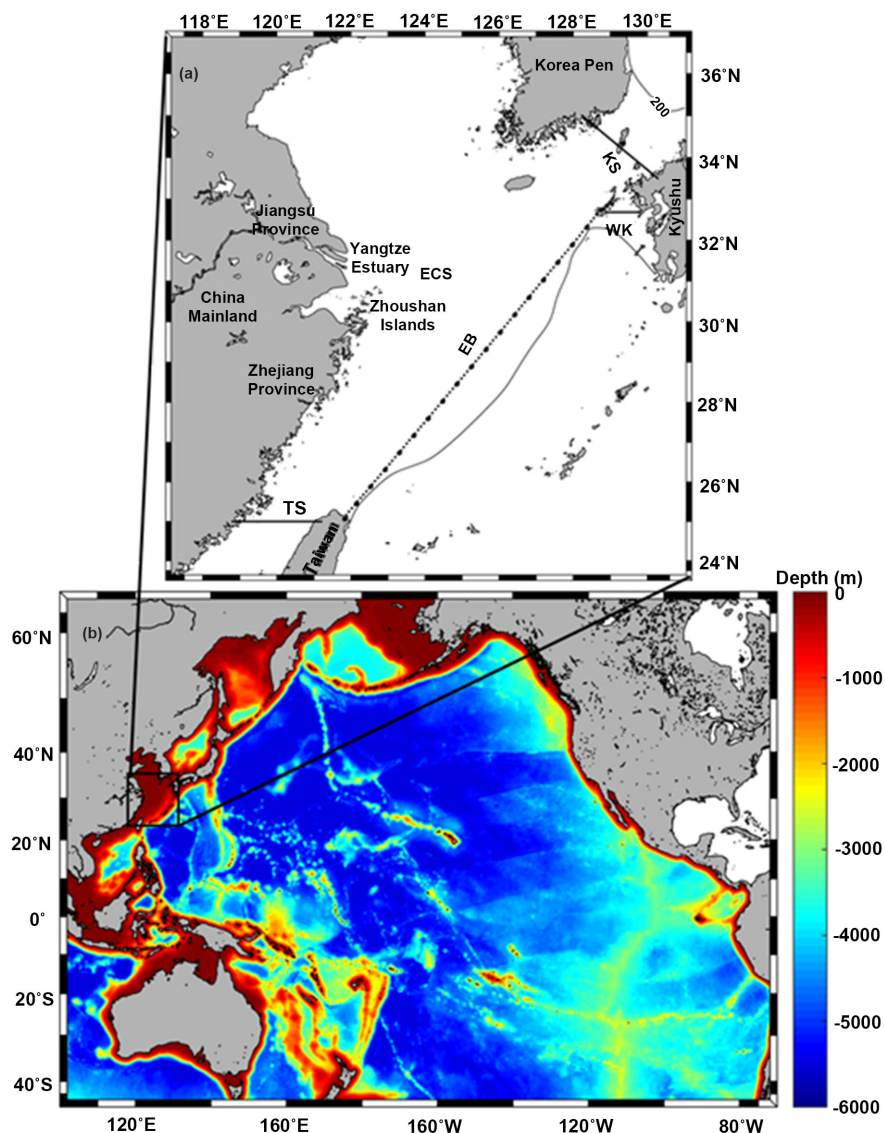


Figure 1. (a) Map of the East China Sea (ECS). TS: the Taiwan Strait; EB: the eastern boundary section of the ECS (EB section); PN: the PN section; WK: the west of the Kyushu; KS: the Korea Strait. The dotted line denotes the EB section, with big dots being plotted every five grid points from the Taiwan coast; (b) Domain of ROMS-CoSiNE model.

from $\sim 26^{\circ}\text{N}$ to $\sim 29^{\circ}\text{N}$ (Zhao & Guo, 2011). The spatial distribution of phosphate transport is consistent with that of the volume transport (Tang et al., 2000; Guo et al., 2006; Lee & Takeshi, 2007). In addition, studies also found that the KIPT shows significant seasonal variability, which is dominated by volume transport (Guo et al., 2006; Zhang et al., 2007; Zhao & Guo, 2011). On the other hand, the variation of KIPT causes changes of ECS biological processes. Based on a three-dimensional coupled biophysical model, Zhao and Guo (2011) reported that the additional nutrients from the Kuroshio would cause an increase in primary production over the ECS shelf from spring to autumn. Using the Regional Ocean Modeling System (ROMS) (Song & Haidvogel, 1994), Yang et al. (2013)

proposed that the phosphate via the Kuroshio causes a high chlorophyll tongue off the coast of Zhejiang province in summer because the high phosphate is transported by a nearshore Kuroshio branch current. This is supported by the result of Wang et al. (2016). However, discussion on the dominant factor of the variation of KIPT and its influence on the ECS biological process on the interannual timescale are limited.

As is well known, the variation and local pattern of the volume transport via Kuroshio intrusion (KIVT) are related to the Kuroshio axis (Sun, 1987; Tang et al., 2000; Liang et al., 2003; Liu et al., 2014). Many studies have reported that when the shoreward (seaward) shift of the Kuroshio axis happens in winter (summer), a weakened (strong) cyclonic eddy appears in the upper layer of the northeast of Taiwan, which induces a stronger (weaker) surface Kuroshio intrusion into the ECS (Su et al., 1990; Tang & Yang, 1993; Tang et al., 2000; Wu et al., 2008, 2014; Oey et al., 2010). However, the relation between the Kuroshio axis and KIPT is not clear. Thus, the objective of this study is to investigate the dominant factor of the variation of KIPT, and to understand how the variation of KIPT affects the ECS biological process and how the change of the Kuroshio axis impacts the KIPT on the interannual timescale.

Due to the lack of continuous *in-situ* data, it is impossible to investigate the variation of KIPT and its relation to the Kuroshio axis on the interannual timescale from observations. Thus, we use a high-resolution physical-biological model with a realistic bathymetry in this study. We defined the volume transport and phosphate transport across the eastern boundary section of the ECS (the EB section) to be the KIVT and KIPT, respectively (Figure 1).

The paper is organized as follows. A brief outline of the physical-biological model (ROMS-CoSiNE) and the *in-situ* data are introduced in Section 2. In Section 3, we compare model simulations with observations and results of previous studies. In Section 4.1, we show the climatology of KIPT, and in Section 4.2, we discuss its interannual variation. The correlation between KIPT and ECS chlorophyll is reported in Section 4.3, and possible mechanism for their relation on the interannual timescale is discussed in Section 4.4. Conclusions are given in Section 5.

2. Model and Data

2.1. Physical-Biological Model

A three-dimensional physical-biological model was used in this study. This model is based on the ROMS, which is a free-surface, terrain-following, primitive equation model to simulate the ocean (Song & Haidvogel, 1994). We configured the ROMS circulation model for the Pacific Ocean (99°E - 70°W, 45°S - 65°N) at a horizontal resolution of about 12.5 km with realistic geometry and topography, which is similar to the configuration used in Wang and Chao (2004) but with a finer resolution. There are 30 vertical levels. Near the two artificial northern and southern walls, a sponge layer with a width of 5° is used at

each wall for temperature, salinity, and nutrients. The treatment of the sponge layer consists of a decay term $\kappa(Q^* - Q)$, namely, $Q = T$ in the temperature equation, $Q = S$ in the salinity equation, and $Q = N$ in the nutrient equation, which restores model variable Q to the observed field Q^* at the two walls. The value of κ varies smoothly from 1/30 day⁻¹ at the wall to zero at 5° from the wall.

The biological component of the model is based on the Carbon, Silicate, Nitrogen Ecosystem (CoSiNE) model by [Chai et al. \(2002\)](#). The CoSiNE model used in this study includes four nutrients (nitrate, ammonium, silicate, and phosphate), two phytoplankton groups (small phytoplankton and diatoms), two grazers (microzooplankton and mesozooplankton), two detritus pools (detritus nitrogen and detritus silicate), total CO₂, and total alkalinity. In this study, we focus on the variation of the phosphate. In the euphotic zone, phosphate and other nutrients is utilized by the two phytoplankton groups, while the phytoplankton's biomass is regulated by zooplankton and their growth rate, which is determined by the Michaelis-Menten type ([Dugdale & Goering, 1967](#)). Below the euphotic zone, sinking particulate organic matters are converted to inorganic nutrients through a regeneration process, in which organic matter decays to ammonium and is then nitrified to nitrate. In addition, the modeled chlorophyll concentration is derived from the phytoplankton biomass concentration ($\text{mmol}\cdot\text{N}\cdot\text{m}^{-3}$), converted to $\text{mg}\cdot\text{m}^{-3}$ using a nominal gram chlorophyll to molar nitrogen ratio of 1.67 ([Chai et al., 2009](#)). The governing equations and all parameters used in this model are described in [Fujii and Chai \(2007\)](#).

In this study, the model was initialized with climatological temperature, salinity, and nutrients from the World Ocean Atlas (WOA) 2005 ([Garcia et al., 2006](#); [Locarnini et al., 2006](#)), and forced by the climatological wind and air-sea fluxes from Comprehensive Ocean-Atmosphere Data Set (COADS). After 10 years of spin up to reach quasi-equilibrium, the model was integrated for the 1997-2016 period, forced with daily air-sea fluxes of momentum, heat, and fresh water derived from the National Centers for Environmental Prediction/the National Center for Atmospheric Research (NCEP/NCAR) reanalysis ([Kalnay et al., 1996](#)). River nutrients were not considered in the model.

2.2. Satellite and *In-Situ* Data

The ECS surface chlorophyll data during July 2002 and December 2016 from the Moderate-resolution Imaging Spectroradiometer (MODIS; <https://oceancolor.gsfc.nasa.gov/>) are used to evaluate the model performance. *In-situ* hydrographic and nutrient data along the PN section from the Japan Meteorological Agency (JMA; <http://www.jodc.go.jp>) are also used to validate the model. Geostrophic current along the PN section was calculated using the hydrographic data for 58 cruises during 1997 and 2009 via the dynamic method ([Hinata, 1996](#)). In our calculation, when the water depth is deeper than 700 m, the reference level is assumed at the 700-m depth; otherwise, the deepest level is

assumed as the reference level in the continental shelf region (Oka & Kawabe, 1998; Guo et al., 2003).

3. Model Validation

3.1. Spatial Distribution and Temporal Evolution of Surface Chlorophyll

We compare the simulated surface chlorophyll with the SeaWiFS data from 1997 to 2009. In **Figure 2(a)** and **Figure 2(b)**, we can see that the distribution of the modeled chlorophyll is similar to that of the satellite data. Both show chlorophyll concentrations decrease from the coast to the open sea. The correlation coefficient between model and observation is 0.89 ($p < 0.01$), which means the model can reproduce the spatial distribution of surface chlorophyll in the ECS. However, the modeled chlorophyll is lower than the satellite data in the coastal area. This discrepancy could result from many factors, including that the nutrients from rivers are not included in the model and there are some inappropriate parameters for the ECS phytoplankton dynamics used in our model. On the other hand, the chlorophyll of the satellite data is often overestimated in the continental shelf because of the strong interferences from suspended sediments, colored dissolved organic matter (CDOM), and reflection from the ocean bottom (Sathyendranath, 2000; Xiu & Chai, 2014). The monthly anomaly time series of the basin-wide chlorophyll is compared with the SeaWiFS data in **Figure 3**. They also show similarity in phase, and their correlation coefficient reaches 0.75. Since we focus on the variation of the chlorophyll and low requirement for the accuracy of the values, the model can be used to investigate the variation of the ECS ecosystem on the interannual time scale.

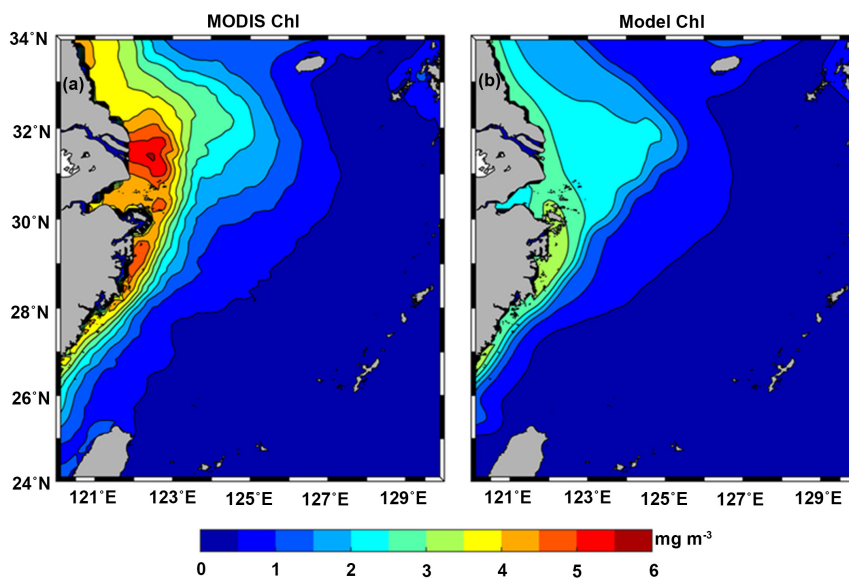


Figure 2. Comparison of surface chlorophyll between model simulation and SeaWiFS observation during 1997-2009. (a) SeaWiFS climatology; (b) Model climatology. Units: $\text{mg}\cdot\text{m}^{-3}$.

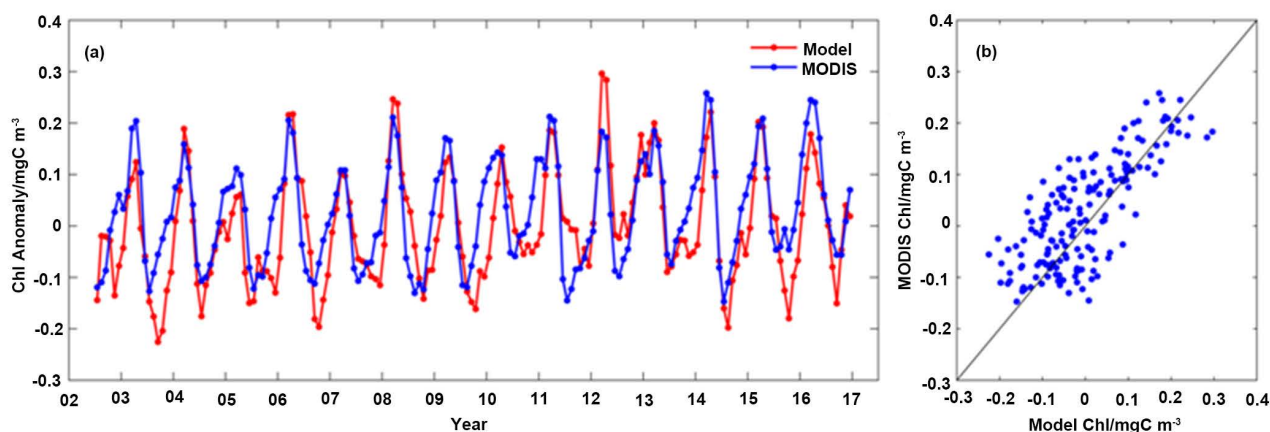


Figure 3. (a) Monthly anomaly time series of model (red line) and SeaWiFs chlorophyll (blue line); (b) Scatter plot of the modeled versus MODIS Chlorophyll. Diagonals in (b) is 1:1 lines. Units: $\text{mg}\cdot\text{m}^{-3}$.

3.2. Mean State along the Pnction

Multi-year averages of model outputs are evaluated against observations. **Figure 4** compares the mean of current velocity, nutrient (nitrate and phosphate) concentration. The spatial pattern of simulated current velocity is consistent with the JMA's, with faster currents in the upper layer of the middle section than on the both sides and in the lower layer (**Figure 4(a)** and **Figure 4(d)**). The model also reasonably reproduces the distribution of nitrate and phosphate concentrations, with high in the bottom water and low in the surface water (**Figure 4(b)**, **Figure 4(c)**, **Figure 4(e)**, and **Figure 4(f)**). The modeled concentration contours tilt to the continental slope as in the observation. In addition, the comparison of nutrient flux along the PN section between simulation and observation is shown in **Figure 5**. The nutrient flux is calculated as the product of current velocity and nutrient concentration. The distribution of observed nitrate and phosphate fluxes are also captured by the model, which all show high value in the subsurface water of the middle PN section. The modeled maximum nitrate and phosphate fluxes reach $6.54 \text{ mmol}\cdot\text{m}^{-2}\cdot\text{s}^{-1}$ and $0.48 \text{ mmol}\cdot\text{m}^{-2}\cdot\text{s}^{-1}$, respectively, which are all slightly smaller than $7.85 \text{ mmol}\cdot\text{m}^{-2}\cdot\text{s}^{-1}$ for nitrate flux and $0.57 \text{ mmol}\cdot\text{m}^{-2}\cdot\text{s}^{-1}$ for phosphate flux of the observations. This discrepancy might come from higher observed nutrient concentration in the lower layer. Moreover, the core of simulated current velocity and nutrient flux are to the west of the observed features. These discrepancies could be due to model error or to insufficient spatial resolution of the observations. The observed data are based on eight stations along the PN section, and at each station only the data at standard depths were recorded (Wei et al., 2013).

3.3. Temporal Evolution of Volume Transport and Phosphate Transport across the PN Section

The yearly anomaly time series of the simulated volume transport (VT), nitrate transport (NT), and phosphate transport (PT) across the PN section are compared

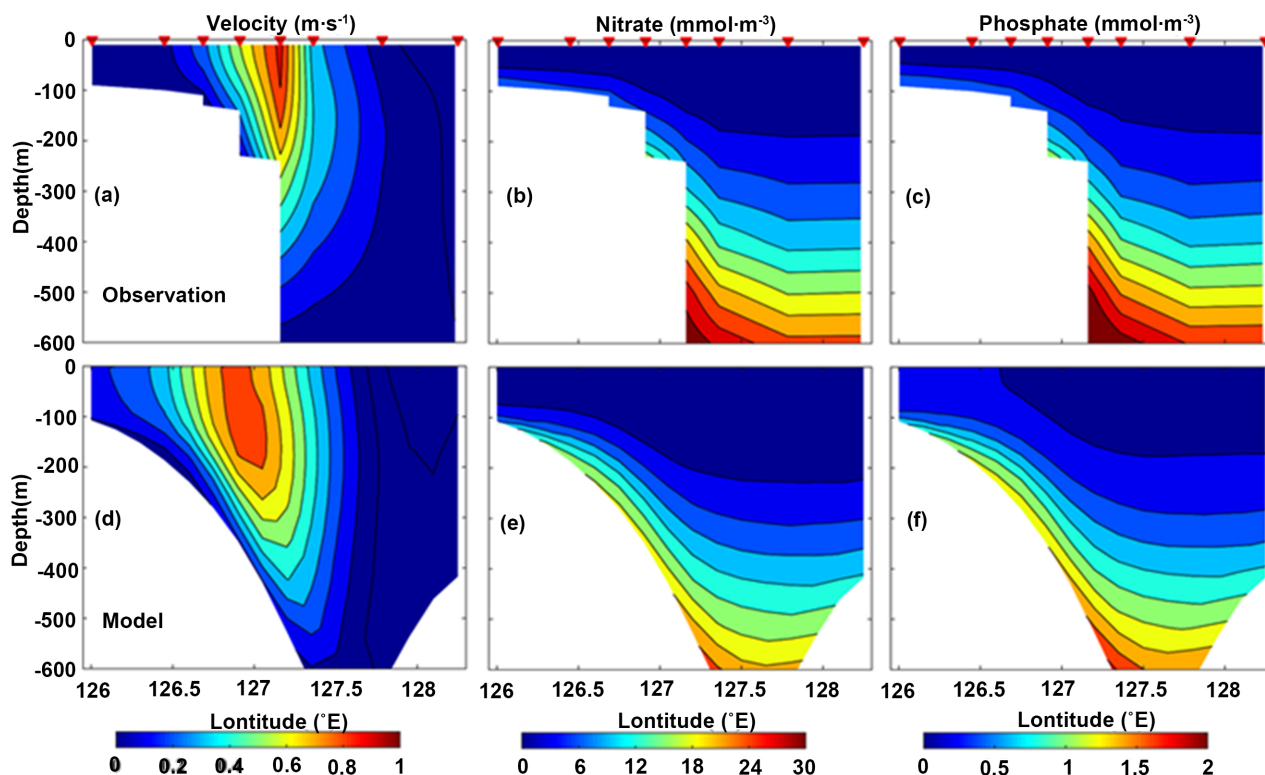


Figure 4. Comparison of current velocity and nutrient concentration (nitrate and phosphate) between JMA observation (1997-2009) (top) and simulated multi-year mean (bottom) along the PN section. Left: Current velocity; middle: nitrate concentration; right: phosphate concentration. The current of JMA observation is computed from geostrophic balance using temperature and salinity observations at stations (red upside-down triangles).

with *in-situ* data in **Figure 6**. The VT, NT, and PT are calculated as the vertical integration of current velocity and phosphate flux from surface to bottom. The variations of VT, NT, and PT across the PN section in model simulation and JMA observations are similar. They have the same phase from 1997 to 2009 (**Figure 6**), especially after 2003. The 20-year-mean model VT, NT and PT across the PN section are about 23.6 Sv, 140.54 $\text{kmol}\cdot\text{s}^{-1}$ and 11.50 $\text{kmol}\cdot\text{s}^{-1}$, respectively. The results are on the same order as estimated values of VT (22.5 Sv), NT (170.8 $\text{kmol}\cdot\text{s}^{-1}$) and PT (12.51 $\text{kmol}\cdot\text{s}^{-1}$) by Guo et al. (2012), in which the current velocity was obtained via the inverse method (Zhu et al., 2006). Overall, the observed current velocity, nutrient concentration, and nutrient flux along the PN section in terms of the mean spatial pattern and interannual variation are reproduced in the model.

3.4. Annual Volume and Nutrient Transports across the Boundary of the ECS

The 20-year mean of VT, NT, and PT through the boundaries (see **Figure 1(a)**) of the ECS based on our model are compared with the estimates by previous studies in **Table 1**. Examining the simulated VT across these boundaries, we can find that they are on the same order to those estimates by using box model and

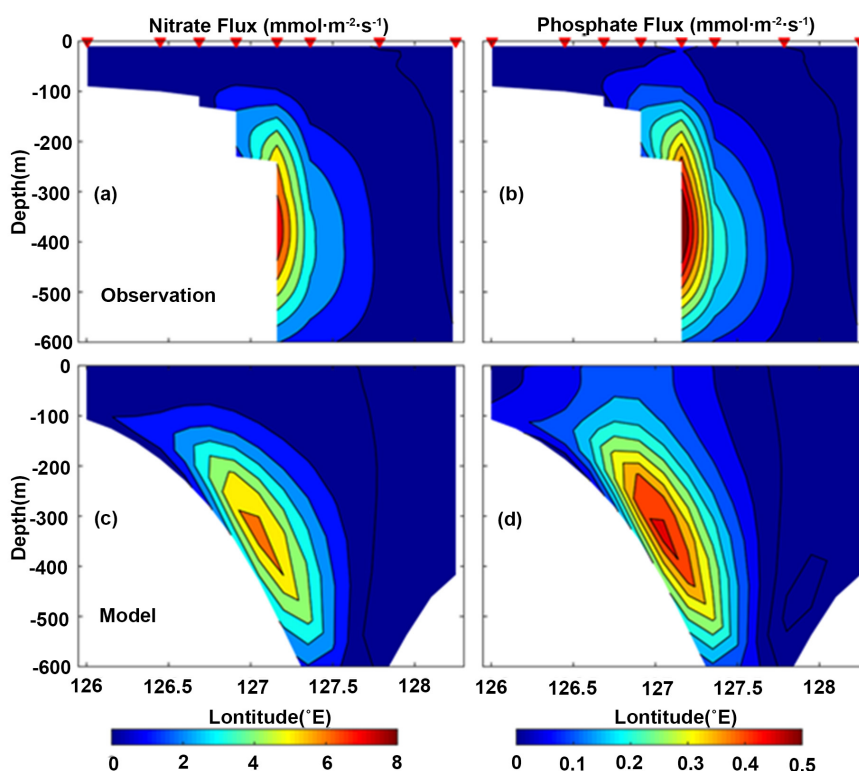


Figure 5. Comparison of nutrient (nitrate and phosphate) flux between JMA observation (1997-2009) (top) and simulated multi-year mean (bottom) along the PN section. Left: nitrate flux; right: phosphate flux. The nutrient flux is calculated as the product of current velocity and nutrient concentration. The red upside-down triangles denote the station of JMA observation.

numerical model of the previous studies (Chen & Wang, 1999; Guo et al., 2006, 2012; Zhang et al., 2007; Zhao & Guo, 2011). However, the VT (0.98 Sv) across the EB section is smaller than that estimated of other studies (1.21 to 1.53 Sv). The selection of cross-section to represent the boundary in different studies is a reason to cause these differences. In some studies, the 200-m isobath was selected as the Eastern Boundary. We selected the EB section as a straight line as shown in Figure 1 to avoid using different vector velocity rotation angles along the EB that might introduce errors. For simulated nutrient transport across these boundaries, they are close to those estimates by Guo et al. (2006, 2012) and Zhang et al. (2007), who obtained these values through biophysical model and box model, respectively, but show significantly different with those reported by Chen and Wang (1999). The incomplete observations along these boundaries in last century may cause a certain amount of error because the estimated transports depend on the data collection. Compared with previous studies, our model result covers longer time period and larger area so that we can obtain more details about the VT, NT and PT across the boundary of the ECS.

Moreover, Table 1 indicates that the net VT across the boundaries is balanced both in previous studies and our study. However, the net NT and PT have positive values, which indicates that there are external nutrients transported into the

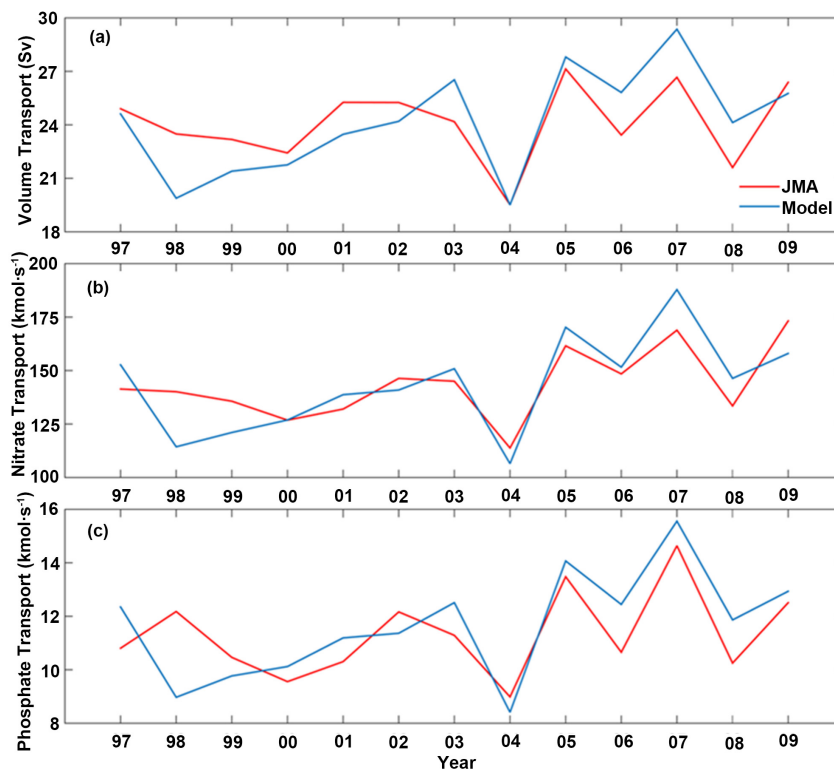


Figure 6. Yearly time series of volume transport (VT) (a), nitrate transport (NT) (b), and phosphate transport (PT) (c) across the PN section between model simulation (blue line) and JMA observations (red line).

ECS. Depending on different methods to obtain those estimates, previous studies show a wide range of the net nutrient transport: 0.98 - 2.60 kmol/s for NT and 0.10 - 0.16 kmol/s for PT. The simulated net NT (1.66 kmol/s) and PT (0.12 kmol/s) lie within the range of estimates by previous studies. Overall, transport estimates from our model are in the range of estimates of previous studies (Table 1) and model output can be used to investigate the variation of phosphate transport via Kuroshio intrusion to the ECS on the interannual timescale.

4. Results and Discussion

4.1. Phosphate Transport via Kuroshio Intrusion across the EB Section

The phosphate flux via Kuroshio intrusion across the EB section into the ECS takes place in the northeast of Taiwan (south of 25.6°N) and southwest of Kyushu (30°N - 31.8°N), while the offshore phosphate transport occurs in the middle of the EB section (25.6°N - 30°N) (Figure 7(a)). The pattern of the 20-year-averaged phosphate flux is basically consistent with that of the current (Figure 7(b)), but the major onshore and offshore phosphate flux are all closer to the lower water (below 100 m) than the current. This is due to low phosphate concentration in the surface water but relatively high phosphate concentration in the bottom water (Figure 7(c)). This feature of the phosphate flux confirms

Table 1. Volume transport (Sv; 1 Sv = 106 m³·s⁻¹), nitrate transport (kmol·s⁻¹), phosphate transport (kmol·s⁻¹) across four major boundary sections and the net transport for the East China Sea, which is obtained by adding the value of each section. Positive value means that the transport is into the East China Sea.

Boundary	VT	NT	PT	Reference	Approach
Taiwan Strait					
	0.36	0.70	0.07	Chen & Wang (1999)	Box model
	1.71	1.40	-	Guo et al. (2006, 2012)	Numerical model ¹
	1.81	6.42	0.41	Zhang et al. (2007)	Box model
	2.12	3.27	0.47	This Study	ROMS-CoSiNE
Korea Strait					
	-1.61	-4.00	-0.25	Chen & Wang (1999)	Box model
	-3.03	-11.40	-	Guo et al. (2006, 2012)	Numerical model ¹
	-3.19	-14.45	-0.96	Zhang et al. (2007)	Box model
	-2.88	-11.23	-1.04	This Study	ROMS-CoSiNE
West of Kyushu					
	-0.14	-	-	Guo et al. (2006)	Numerical model ¹
	-0.15	-	-	Liu et al. (2014)	ROMS model
	-0.21	-0.64	-0.07	This Study	ROMS-CoSiNE
Kuroshio or EB Section					
	1.21	4.70	0.34	Chen & Wang (1999)	Box model
	1.46	12.60	-	Guo et al. (2006, 2012)	Numerical model ¹
	1.35	9.01	0.65	Zhang et al. (2007)	Box model
	1.53	9.40	0.70	Zhao & Guo (2011)	Numerical model ¹
	0.98	10.26	0.76	This Study	ROMS-CoSiNE
Net Balance					
	-0.04	1.40	0.16	Chen & Wang (1999)	Box model
	0.00	2.60	-	Guo et al. (2006, 2012)	Numerical model ¹
	-0.03	0.98	0.10	Zhang et al. (2007)	Box model
	0.01	1.66	0.12	This Study	ROMS-CoSiNE

¹The numerical model used by Guo et al. (2006, 2012) and Zhao and Guo (2011) is a physical-biological model, which is based on the Princeton Ocean Model and the biological part of NORWECOM.

that the Kuroshio subsurface and bottom waters are important sources for the ECS phosphate (Chen & Chung, 1990, 1995; Ito et al., 1994; Chen & Wang, 1999; Yang et al., 2011). Further, **Figure 8** confirms the above analysis but the inflow ranges of volume and phosphate transport via Kuroshio intrusion into the ECS (namely, KIVT and KIPT) in the northeast of Taiwan are smaller than those in the southwest of Kyushu, although the maxima of current and phosphate flux are all

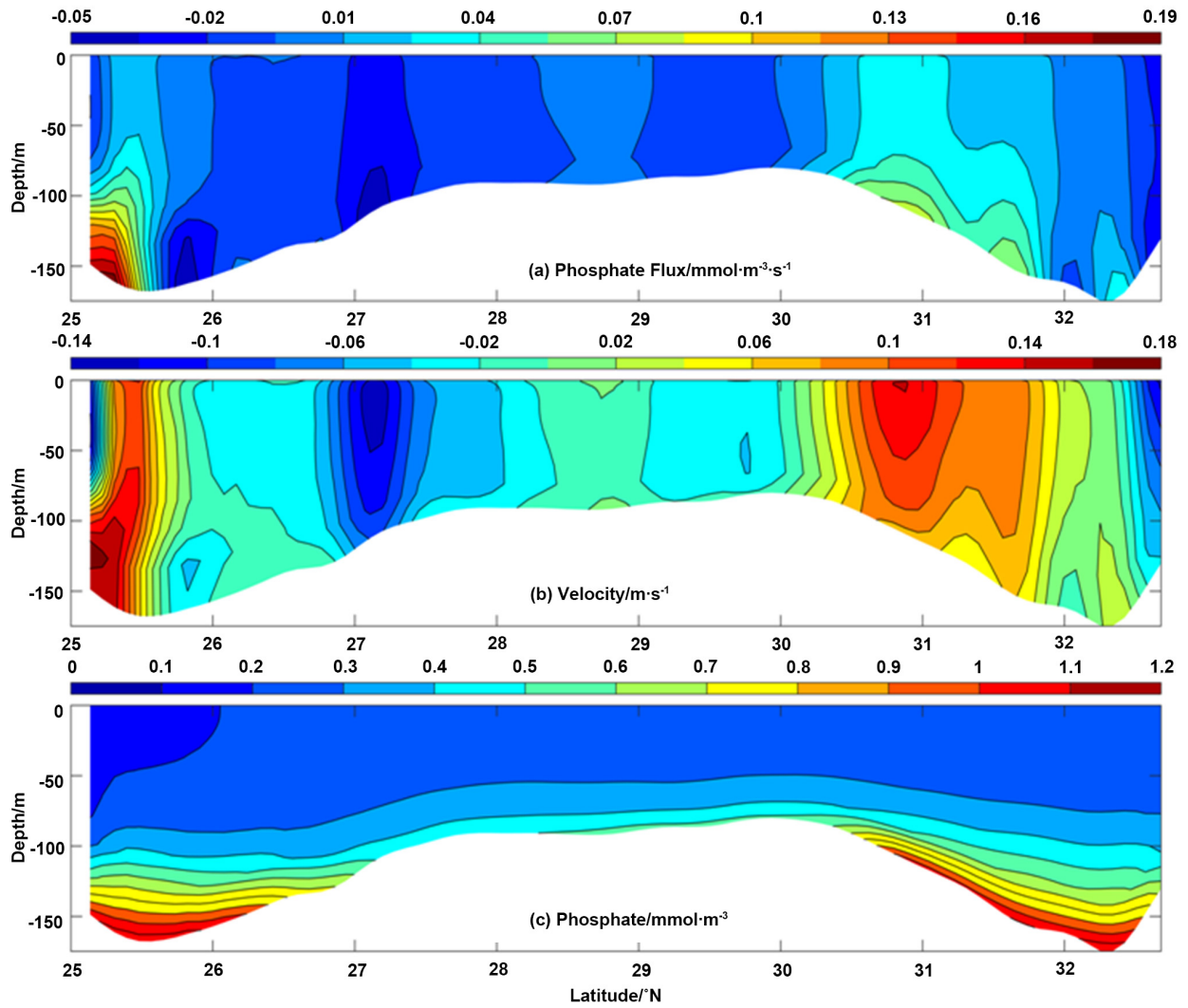


Figure 7. Distribution of 20-year-averaged phosphate flux (a), current velocity (b), and phosphate concentration (c) along the eastern boundary section of the East China Sea. For the phosphate flux and current velocity, positive value means that the flux is into the East China Sea. Contour interval is 0.01 mmol·m⁻³·s⁻¹, 0.01 m·s⁻¹, and 0.01 mmol·m⁻³ for phosphate flux, current velocity, and phosphate concentration, respectively. The locations of grid points are shown in **Figure 1(a)**.

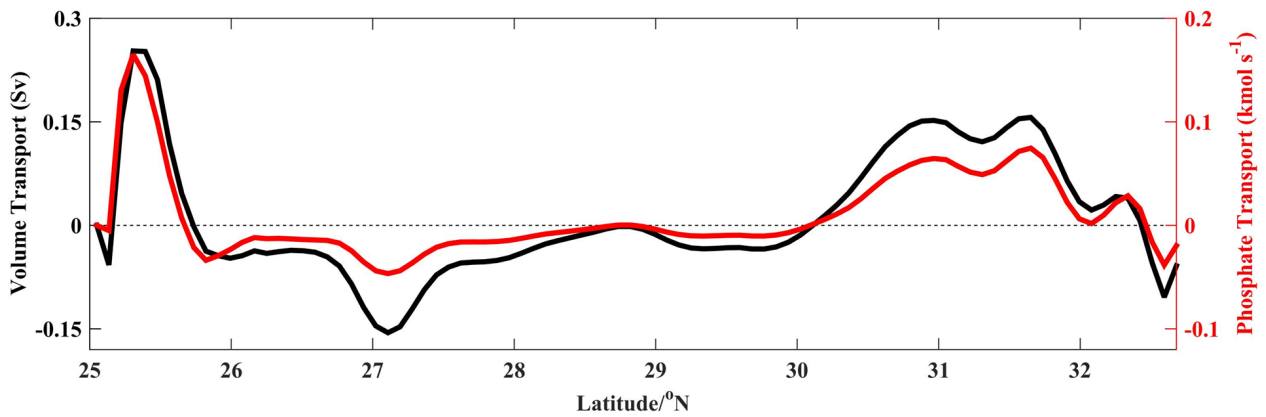


Figure 8. Twenty-year-averaged depth-integrated volume transport (black line) and phosphate transport (red line) for the eastern boundary section of the East China Sea. The locations of grid points are shown in **Figure 1(a)**.

in the northeast of Taiwan. Also in **Figure 8**, the similarity between these two curves means KIVT and KIPT are basically similar. This is different from some studies (Guo et al., 2006; Zhao & Guo, 2011; Liu et al., 2014), which reported wider ranges of Kuroshio intrusion in the northeast of Taiwan. This discrepancy could be also due to selection of cross-section to represent the Kuroshio intrusion into the ECS. The bottom line is these studies also reported that the current and phosphate flux into the ECS mainly occur in the above two regions.

4.2. Interannual Variation of KIPT across the EB Section

The KIVT shows significant interannual variability (Guo et al., 2006; Liu et al., 2014; Yang et al., 2017), but the variation of the KIPT on the interannual timescale and its dominant factors is still unclear. To investigate this, we obtained monthly interannual component (MIC) of KIPT via the following procedures: 1) removing the seasonal cycle and linear trend from the original monthly phosphate transport across the EB section, and 2) applying a 13-month running mean to the monthly result from step 1 (Soeyanto et al., 2014). Meanwhile, to understand the dominant factors of KIPT on the interannual timescale, the MIC of KIVT and the section-averaged phosphate concentration were obtained by using the above method.

Firstly, we display the time series of the MIC KIPT and KIVT across the EB section, and the section-averaged phosphate concentration in **Figure 9**, along with their power spectral analysis. **Figure 9(a)** shows that the KIPT has significant interannual variation. High phosphate transport occurred in the years of 1999-2001 and 2012-2013, and low transport occurred in the years of 1997, 2003, 2005, and 2007. The standard deviation (STD) of the MIC KIPT is 0.17 kmol/s, which is nearly half of the total STD (0.40 kmol/s). The variability of the KIPT is closer to that of KIVT through the EB section (**Figure 9(c)**) but also similar to that of section-averaged phosphate concentration (**Figure 9(e)**). The correlation coefficient between time series of KIVT and KIPT is 0.82, which is also more than that between time series of KIPT and the section-averaged phosphate concentration (0.70). This result shows that the MIC KIPT is dominated by MIC KIVT, but it is also affected by phosphate concentration. Furthermore, spectral analyses on the MIC KIPT, KIVT all show periods on the interannual timescale: about ~2 years and ~4 years at the 90% confident level (**Figure 9(b)**, **Figure 9(d)**, and **Figure 9(f)**) but that of section-averaged phosphate concentration is about ~2.5 years and ~3.5 years. The reason for this variation of phosphate concentration is depending on the water property along the entire EB section, which is decided by the Kuroshio water and offshore shelf water.

To confirm the above analyses and investigate the localized variation of the KIPT, we decompose the variance of MIC phosphate flux along the EB section into six terms according to the method of Guo et al. (2012). As is well known, phosphate flux (c) is the product of current velocity (V) and phosphate concentration (P). If we separate both velocity and phosphate concentration into mean part (V and P) and anomaly part (V' and P'), F can be expressed as follows,

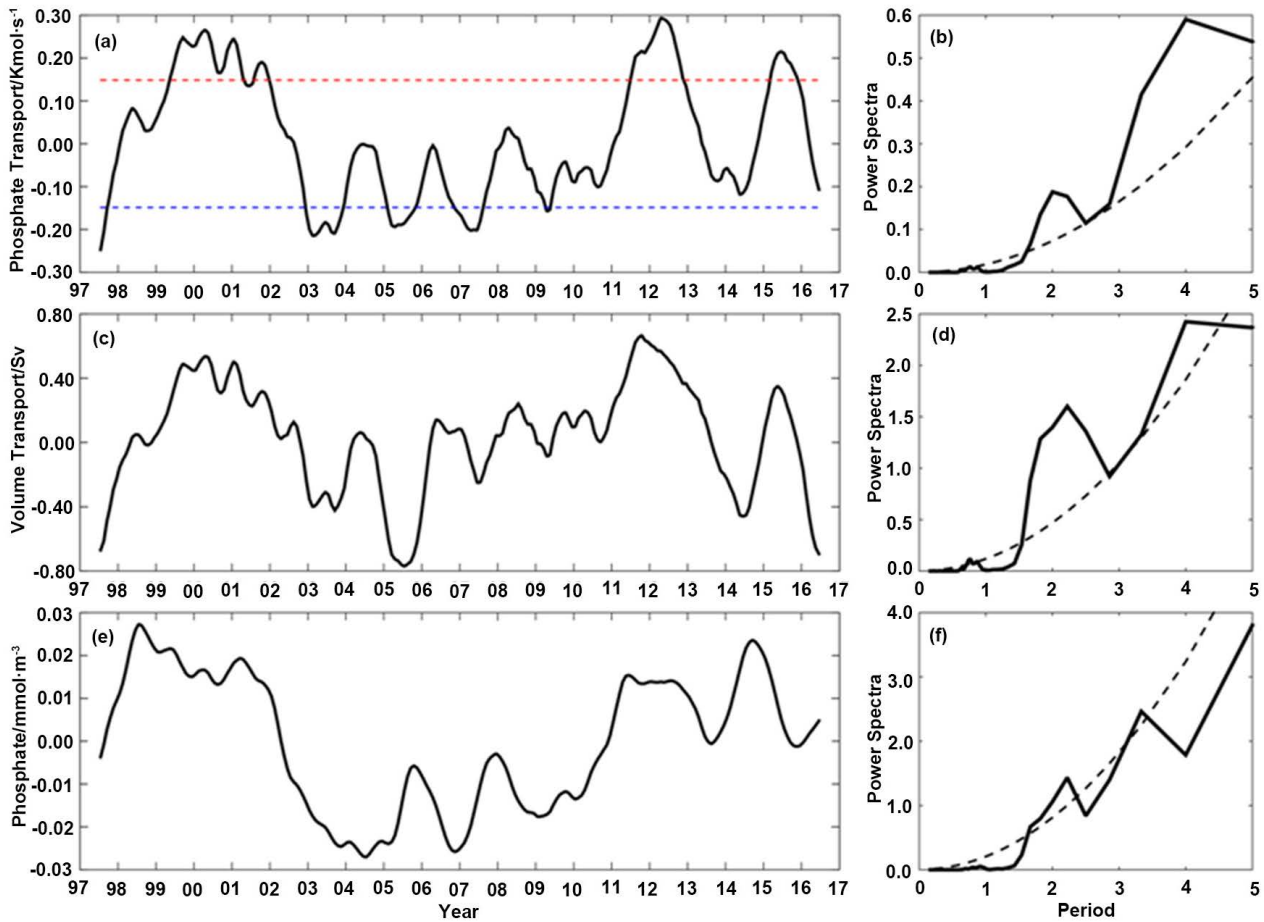


Figure 9. Monthly interannual component (MIC) of (a) the total KIPT through the EB section, (c) the total KIVT through the EB section, and (e) the section-averaged phosphate concentration with their power spectral density shown on the right. The red and blue dashed lines in (a) represent the 20-year-averaged value of KIPT plus and minus their one standard deviation. In (b), (d), and (f), the dashed line denotes the 90% confident level of the power spectral density.

$$F = (\bar{V} + V') \times (\bar{P} + P')$$

Then, the covariance of phosphate flux can be separated into six components,

$$\sigma_F^2 = \bar{P}^2 \sigma_V^2 + \bar{V}^2 \sigma_P^2 + 2\bar{P}\bar{V}\sigma_{PV}^2 + 2\bar{P}\sigma_{VG}^2 + 2\bar{V}\sigma_{PG}^2 + \sigma_G^2$$

where σ_F^2 is the variance of phosphate flux. $\bar{P}^2 \sigma_V^2$ is the product of mean phosphate concentration and variance of velocity; $\bar{V}^2 \sigma_P^2$ is the product of mean velocity and variance of phosphate concentration; $2\bar{P}\bar{V}\sigma_{PV}^2$ is the product of mean velocity, mean phosphate concentration, and covariance of velocity and phosphate concentration. G is the product of the anomaly of velocity and phosphate concentration. Thus, $2\bar{P}\sigma_{VG}^2$ is the product of mean phosphate concentration and covariance of velocity and G . $2\bar{V}\sigma_{PG}^2$ is the product of mean velocity and covariance of phosphate concentration and G . σ_G^2 is the variance of G .

Figures 10(a)-(d) show the terms σ_F^2 , $\bar{P}^2 \sigma_V^2$, $\bar{V}^2 \sigma_P^2$, $2\bar{P}\bar{V}\sigma_{PV}^2$ and of the above equation, and the other three terms on the right-hand side of the equation are negligible. As expected, the variance of MIC phosphate flux has a higher

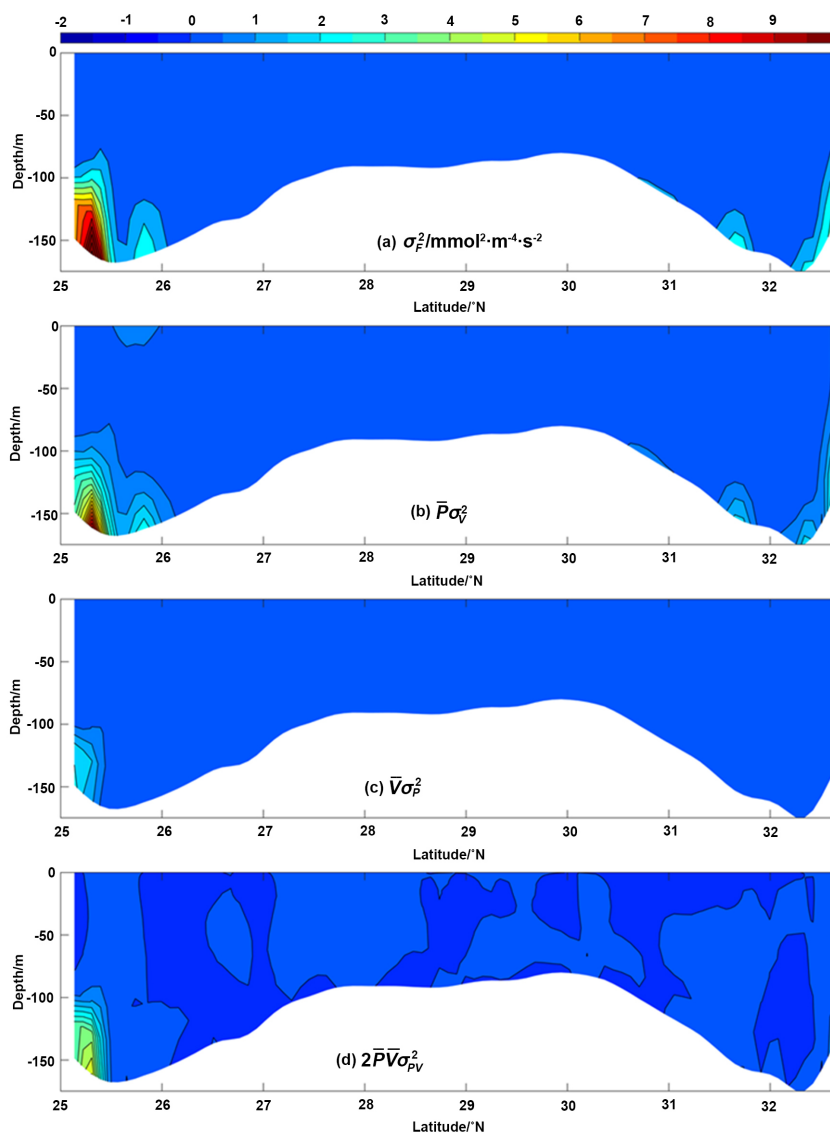


Figure 10. Variance of the interannual component of phosphate flux (a) and its decomposed terms of $\bar{P}^2\sigma_V^2$, $\bar{V}^2\sigma_P^2$, and $2\bar{P}\bar{V}\sigma_{P_V}^2$ (b-d), following the variance equation at each grid along the eastern boundary section of the East China Sea. For convenience, the value has been magnified 10^4 times. Units: $\text{mmol}^2 \cdot \text{m}^{-4} \cdot \text{s}^{-2}$.

value in the near-bottom water south of 26°N than that in the other region of the EB section (**Figure 10(a)**). It indicates that the MIC KIPT has significant variation in the northeast of Taiwan. For the three terms on the right-hand side of Equation (2), a pronounced feature is that the variance of these terms show high value in the northeast of Taiwan and the value of the term $\bar{P}^2\sigma_V^2$ makes up a major part of the variance of MIC phosphate flux (σ_F^2). However, the terms $\bar{V}^2\sigma_P^2$ and $2\bar{P}\bar{V}\sigma_{P_V}^2$ (**Figure 10(c)** and **Figure 10(d)**) are not small enough to be negligible. These results suggest that the variation of the MIC phosphate flux is dominated by the term of current velocity, while it is also affected by the term of phosphate concentration and the covariance of current velocity and phos-

phate concentration. The above analysis shows that the interannual variation of the KIPT is dominated by the current velocity of Kuroshio intrusion (or current velocity) but also be influenced by that of phosphate concentration in the Kuroshio intrusion water.

4.3. Relationship between KIPT and ECS Chlorophyll

To explore the influence of the KIPT on the ECS chlorophyll at the interannual timescale, the spatial distribution of correlation coefficient between the two at each grid from 1997 to 2016 is displayed in **Figure 11**. There is significant positive correlation in the region around (32°N, 124.5°E) and the offshore area of the north Yangtze Estuary and Hangzhou Bay, especially around the Zhoushan Islands, which is a well-known fishing ground (**Figure 11**). On the other hand, the most significant negative correlation occurs in the north of Taiwan, which is a major passage of phosphate transport from the northeast of Taiwan to the Zhoushan Islands (Yang et al., 2011, 2012). The other area of negative correlation is in the area around (29°N, 125°E), where the primary production is limited by nitrate. The above results indicate that when there is high phosphate transport across the EB section, chlorophyll tends to be higher around the Zhoushan Islands and lower in the outer shelf region.

To examine the above analysis, chlorophyll anomaly is shown in **Figure 12** for the periods when the MIC KIPT is more than its mean plus one standard deviation or less than its mean minus one standard deviation, as indicated in **Figure 9(a)**. When the MIC KIPT is in high intrusion period, it is evident that chlorophyll increases in the ECS inner shelf, especially around the Zhoushan Islands. The increased chlorophyll concentration is more than $0.4 \text{ mg}\cdot\text{m}^{-3}$. However, the slightly decreased chlorophyll occurs in the north of Taiwan and the area around (29°N, 125°E) (**Figure 12(a)**), which is corresponding to the region of negative correlation between KIPT and chlorophyll (**Figure 11**). It means there is more phosphate being transported by the Kuroshio to the coastal region of the ECS but less phosphate is used by phytoplankton in the north of Taiwan and outer shelf of the middle ECS. On the other hand, when the MIC KIPT is in a low intrusion period, there is essentially decreased chlorophyll in the ECS shelf, especially in the Zhejiang coastal areas (**Figure 12(b)**). The distribution of chlorophyll anomalous is similar in spatial pattern but opposite in sign for the periods with high and low KIPT intrusions.

4.4. Possible Mechanism for MIC KIPT Influence on ECS Chlorophyll

From the above analyses, the variation of the MIC KIPT is dominated by the MIC KIVT. Many studies showed that the KIVT into the ECS has a close relation with the shoreward-seaward movement of the Kuroshio axis (Tang et al. 1999, 2000; Wu et al. 2008, 2014; Liu et al., 2014). Thus, we will investigate whether the KIPT is influenced by the movement of the Kuroshio axis. To

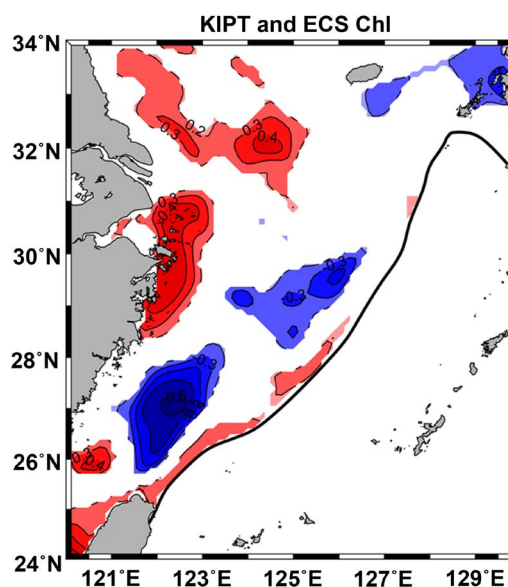


Figure 11. Correlation coefficient between the phosphate transport through the EB section and the ECS chlorophyll for the period from 1997 to 2016. Only the shelf region (water depth less than 200 m) where the correlation coefficient is significant at 90% confidence level is shown.

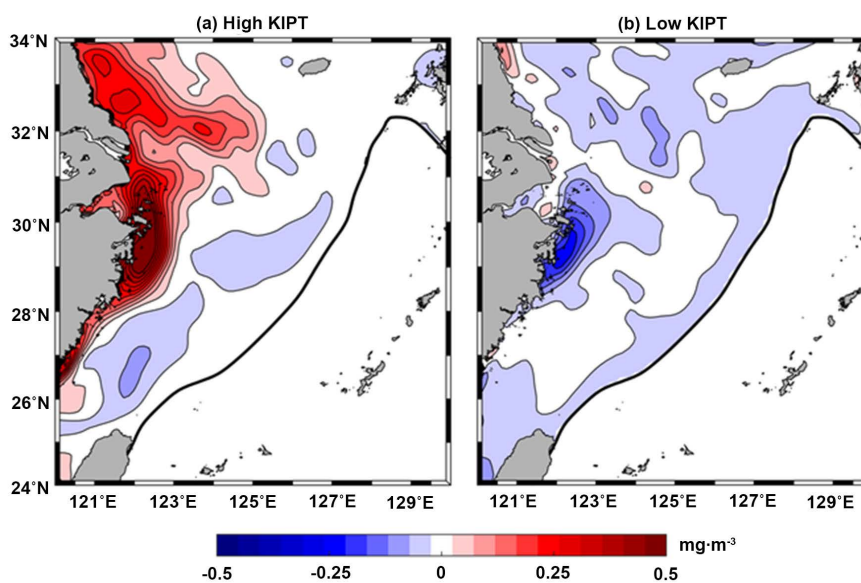


Figure 12. Surface chlorophyll anomaly for the periods when the phosphate transport is more than the mean plus one standard deviation (a) and less than the mean minus one standard deviation (b). The two periods are shown in [Figure 6\(a\)](#). Only the shelf region of the ECS (depth < 200 m) is shown here. Units: $\text{mg}\cdot\text{m}^{-3}$.

address this, we define the longitude of the maximum velocity along the PN section as the index of the Kuroshio axis (KAI), to examine its relationship with the MIC KIPT. The normalized time series of the KAI and KIPT are shown in [Figure 13\(a\)](#). They have opposite phase in the entire 20 year, which suggests that the shoreward shift of Kuroshio axis will accompany the more KIPT into

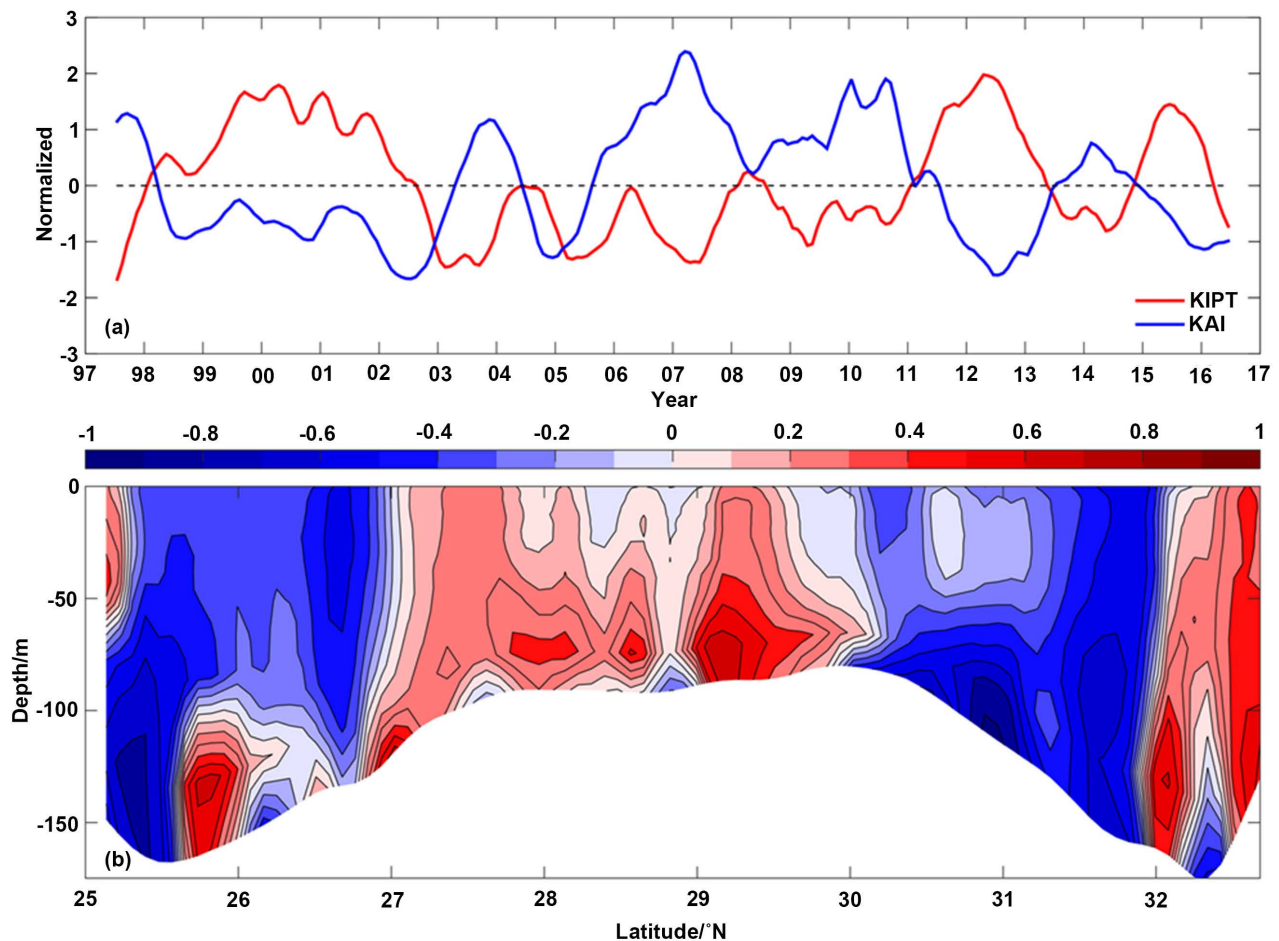


Figure 13. (a) The normalized time series of the interannual component of the Kuroshio axis index and KIPT; (b) Correlation coefficients between the interannual component of the Kuroshio axis index and the phosphate flux along the eastern boundary of the East China Sea. The Kuroshio axis index is defined as the longitude of the maximum velocity along the PN section.

the ECS. The correlation coefficients between the MIC phosphate flux at each grid along the EB section and the KAI show significant negative values in the subsurface water of major Kuroshio intrusion region (south of 25.6°N and 30°N - 31.8°N), northeast of Taiwan and southwest of Kyushu, but show basically positive values in the outflow region, the middle part of EB section (27°N - 30°N) (Figure 13(b)). It means that the shoreward (seaward) movement of the Kuroshio axis is associated with the increased (decreased) KIPT in the subsurface water. Thus, the change of ECS chlorophyll may be affected by the Kuroshio axis migration, through regulating the variation of the KIPT on the interannual timescale.

The shoreward-seaward shift of the Kuroshio axis will intensify or suppress an upper-layer cyclonic eddy in the northeast of Taiwan, and regulate the Kuroshio intrusion into the ECS (Liu et al., 1992; Tang et al., 1999, 2000; Wu et al., 2008, 2014; Liu et al., 2014; Wang et al., 2016). Our simulated results, however, show that the phosphate intrusion mainly happens in the near-bottom water. Therefore, the bottom velocity anomaly is shown in Figure 14 for the high and low

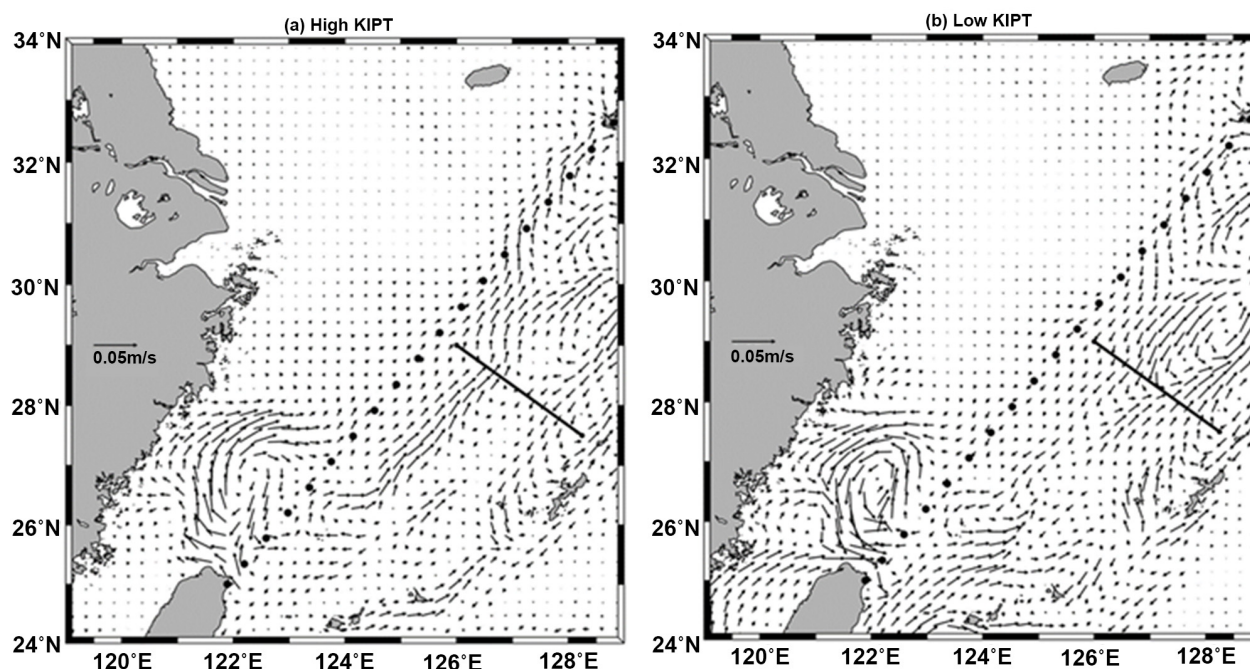


Figure 14. The lower velocity anomaly for the periods when the phosphate transport is more than the mean plus one standard deviation (a) and less than the mean minus one standard deviation (b). The two periods are shown in **Figure 9(a)**. The bottom velocity is selected as the lower velocity in the shelf area (depth < 200 m), but the velocity of 200 m is selected as the lower velocity in other area (depth > 200 m).

phosphate intrusion periods to explore the influence of Kuroshio axis change on the KIPT. The high and low phosphate intrusion periods are the same as those used in **Figure 12**. In **Figure 14(a)**, we can find that when the KIPT intensifies, an anticyclonic eddy-like bottom velocity anomaly emerges northeast of Taiwan. The southern part of the anticyclonic eddy-like bottom velocity anomaly is close to the south of EB section, which is a major intrusion region. It indicates that the bottom shoreward flow with rich phosphate from the Kuroshio intrusion is stronger than the mean state, and intrudes farther westward into the ECS inner shelf. Meanwhile, the current will carry more phosphate from the Kuroshio water to arrive in the area around the Zhoushan Islands and Yangtze Estuary. The additional bottom phosphate intrusion can be used by phytoplankton through the coastal upwelling to increase chlorophyll (**Chen et al., 2004; Qiao et al., 2006; Yang et al., 2011**). However, the increased phosphate intrusion into the ECS coastal region does not occur southwest of Kyushu.

The contrary pattern of the bottom velocity anomaly happens in the low intrusion period (**Figure 14(b)**). A cyclonic eddy-like velocity anomaly takes place northeast of Taiwan, and the shoreward transport decreases, which gives decreased chlorophyll around the Zhoushan Islands and Yangtze Estuary. Meanwhile, we can also find that the increased inflow from the Taiwan Warm Current take place and supplies some phosphate along the Fujian coasts (**Yang et al., 2018a**). This can explain that the chlorophyll in the north of Taiwan is not obviously decreased in **Figure 12(b)**. Other than that, the decreased intrusion happening

southwest of Kyushu is not associated with a cyclonic eddy-like velocity difference. Combined with **Figure 14(a)**, the intrusion phosphate southwest of Kyushu plays a small role in the ECS biological process, because its major part will flow out to the ECS through the Korea Strait (Lie et al., 1998; Guo et al., 2006). **Figure 14** also shows that when the more KIPT is into the ECS, the current velocity of 200 m will increase in the shore side of the PN section but decrease in the offshore side. Conversely, the velocity of 200 m increases in the offshore side of the PN section but decreases in the shore side when the less KIPT is into the ECS. The above analyses indicate that the onshore (offshore) shift of the Kuroshio axis is accompanied by increased (decreased) KIPT northeast of Taiwan, which induces anticyclonic (cyclonic) eddy-like velocity anomaly in the bottom, making the phosphate from the Kuroshio water intrude further to (farther away from) the coastal area and affect chlorophyll in the ECS.

Though this process can link the movement of the Kuroshio axis to the change of ECS chlorophyll, it is still not clear why the variation of the Kuroshio causes phosphate transport into the coastal area. According to the topographic beta spiral theory (Yang et al., 2018b), the Kuroshio intrusion depends on the velocity angle ($\theta = \tan^{-1}(u/v)$), which changes with depth and is regulated by bottom upwelling (w_B). When $w_B > 0$, the horizontal current rotates in the form of left-hand spiral, which makes the Kuroshio subsurface water intrude farther westward than the Kuroshio surface water. When $w_B < 0$, the subsurface water intrudes less than the surface water. The simulated result shows that the bottom upwelling along the EB section is positive in the northeast of Taiwan, which is consistent with this theory. However, the bottom upwelling is not all positive in the southwest of Kyushu. It means that the phosphate intrusion in the southwest of Kyushu is not controlled by the Kuroshio subsurface water. To investigate the variation of bottom upwelling, the bottom upwelling along the EB section in high and low intrusion periods are shown in **Figure 15**. As expected, when there is high (low) KIPT into the ECS, the bottom upwelling is stronger (weaker) than that of the 20-year average, happening in the northeast of Taiwan, but the variation is not significant in the southeast of Kyushu. More specifically, the upwelling increases by about $5.5 \times 10^{-4} \text{ m}\cdot\text{s}^{-1}$ around the northeast of Taiwan in high intrusion period but decreases by about $4.8 \times 10^{-4} \text{ m}\cdot\text{s}^{-1}$ in low intrusion period. However, no matter which period, the change of upwelling around southwest of Kyushu is far less than that around the northeast of Taiwan which might explain why there is stronger intrusion in the northeast of Taiwan than in the southwest of Kyushu. Overall, strong upwelling is associated with strong topographic beta spiral, and more phosphate is transported into the coastal area as a result.

5. Conclusion

Using the three-dimensional Pacific physical-biological model of ROMS-CoSiNE, we investigated the variation of nutrient transport via Kuroshio intrusion and chlorophyll in the ECS. The model is capable of reproducing the observed

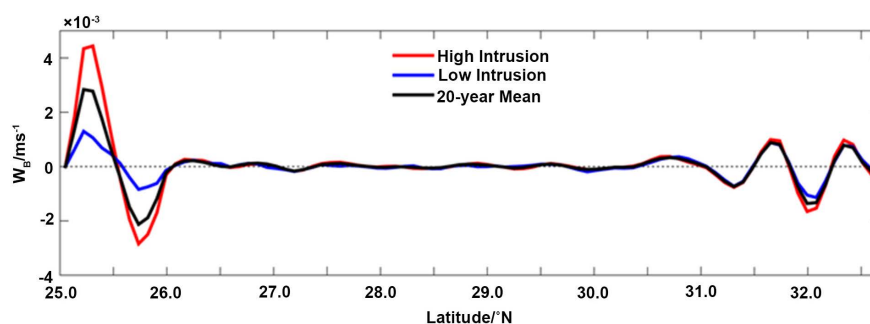


Figure 15. Bottom upwelling velocity of 20-year mean (black line), high intrusion period (red line), and low intrusion period (blue line) at each grid of the eastern boundary section of the East China Sea (the EB section). The high and low intrusion periods are shown in **Figure 6(a)**. The locations of grid points are shown in **Figure 1**.

multi-year-averaged current velocity, nutrient flux, and interannual variation of nutrient transport across the PN section. The model simulation also shows that the total phosphate transport across the eastern boundary of the ECS enters the ECS, and the major intrusion regions are the northeast of Taiwan and southwest of Kyushu; the total phosphate transport across the eastern boundary of the ECS is similar to the Kuroshio intrusion volume transport. For the interannual variation of phosphate transport across the eastern boundary of the ECS, large variability occurs in the near-bottom water northeast of Taiwan. In addition, the variation of volume transport is found to be the major cause for the interannual variation of phosphate transport, after we decompose the variance of phosphate transport into six terms.

The phosphate transport across the eastern boundary of the ECS can cause a significant change in the biological process in the region. High phosphate transport along the eastern boundary is associated with increased surface chlorophyll around the Zhoushan Islands and Yangtze Estuary, but with decreased chlorophyll in the outer shelf. The variation of the Kuroshio axis and the upwelling along the eastern boundary might play crucial roles in this connection. When the Kuroshio axis is closer to the ECS shelf, the bottom upwelling along the eastern boundary will be enhanced, which causes an anticyclonic eddy-like anomaly in the bottom water northeast of Taiwan. Thus, more phosphate transport occurs northeast of Taiwan; and phosphate intrudes farther northwestward to arrive around the Zhoushan Islands and Yangtze Estuary, which induces the increase of surface chlorophyll around the region.

Phosphate is essential to all modern forms of life. Phosphate is also a key biological cornerstone. It is an important source of DNA and adenosine triphosphate (ATP), an energy source that drives cells. This chemical is involved in metabolism, the chemical reaction of life, and no phosphate, life is hard to imagine. At the same time, however, excessive phosphate also causes environmental pollution. The various properties of the ocean and the various environments of the ocean have a major impact on the existence and distribution of various marine organisms and sediments. As the global environment gradually deteriorates, the

problem of marine environmental pollution has become a concern of the society. Continued research can provide a scientific basis for this.

Acknowledgements

This research is funded by National Key Research Project 2016YFC1401600 and State Ocean Administration Project 201505003.

Conflicts of Interest

The authors declare no conflicts of interest regarding the publication of this paper.

References

- Chai, F., Dugdale, R., Peng, T.-H., Wilkerson, F., & Barber, R. (2002). One-Dimensional Ecosystem Model of the Equatorial Pacific Upwelling System. Part I: Model Development and Silicon and Nitrogen Cycle. *Deep Sea Research Part II: Topical Studies in Oceanography*, 49, 2713-2745. [https://doi.org/10.1016/S0967-0645\(02\)00055-3](https://doi.org/10.1016/S0967-0645(02)00055-3)
- Chai, F., Liu, G., Xue, H., Shi, L., Chao, Y., Tseng, C.-M., Chou, W.-C., & Liu, K.-K. (2009). Seasonal and Interannual Variability of Carbon Cycle in South China Sea: A Three-Dimensional Physical-Biogeochemical Modeling Study. *Journal of Oceanography*, 65, 703-720. <https://doi.org/10.1007/s10872-009-0061-5>
- Chen, C. T. A., & Wang, S. L. (1999). Carbon, Alkalinity and Nutrient Budgets on the East China Sea Continental Shelf. *Journal of Geophysical Research: Oceans*, 104, 20675-20686. <https://doi.org/10.1029/1999JC900055>
- Chen, C., Ruo, R., Paid, S., Liu, C.-T., & Wong, G. (1995). Exchange of Water Masses between the East China Sea and the Kuroshio off Northeastern Taiwan. *Continental Shelf Research*, 15, 19-39. [https://doi.org/10.1016/0278-4343\(93\)E0001-O](https://doi.org/10.1016/0278-4343(93)E0001-O)
- Chen, C.-T. A. (2008). Distributions of Nutrients in the East China Sea and the South China Sea Connection. *Journal of Oceanography*, 64, 737-751. <https://doi.org/10.1007/s10872-008-0062-9>
- Chen, R. S., & Chung, Y. C. (1990) Sedimentation Rates in the Western Philippine Sea. *Terrestrial, Atmospheric and Oceanic Sciences*, 1, 111-125. <http://www.airitilibrary.cn/Publication/alDetailedMesh?DocID=10170839-199003-1-1-111-125-a> [https://doi.org/10.3319/TAO.1990.1.1.111\(O\)](https://doi.org/10.3319/TAO.1990.1.1.111(O))
- Chen, Y.-L. L., Chen, H.-Y., Gong, G.-C., Lin, Y.-H., Jan, S., & Takahashi, M. (2004). Phytoplankton Production during a Summer Coastal Upwelling in the East China Sea. *Continental Shelf Research*, 24, 1321-1338. <https://doi.org/10.1016/j.csr.2004.04.002>
- Dugdale, R., & Goering, J. (1967). Uptake of New and Regenerated Forms of Nitrogen in Primary Productivity. *Limnology and Oceanography*, 12, 196-206. <https://doi.org/10.4319/lo.1967.12.2.0196>
- Fujii, M., & Chai, F. (2007). Modeling Carbon and Silicon Cycling in the Equatorial Pacific. *Deep Sea Research Part II: Topical Studies in Oceanography*, 54, 496-520. <https://doi.org/10.1016/j.dsr2.2006.12.005>
- Garcia, H., Locarnini, R., Boyer, T., & Antonov, J. (2006). World Ocean Atlas 2005, Vol. 4: Nutrients (Phosphate, Nitrate, Silicate). In S. Levitus (Ed.), *NOAA Atlas NESDIS 64* (396 p.). Washington DC: U.S. Government Printing Office.
- Guo, X., Hukuda, H., Miyazawa, Y., & Yamagata, T. (2003). A Triply Nested Ocean Mod-

- el for Simulating the Kuroshio—Roles of Horizontal Resolution on JEBAR. *Journal of Physical Oceanography*, *33*, 146-169. [https://doi.org/10.1175/1520-0485\(2003\)033<0146:ATNOMF>2.0.CO;2](https://doi.org/10.1175/1520-0485(2003)033<0146:ATNOMF>2.0.CO;2)
- Guo, X., Miyazawa, Y., & Yamagata, T. (2006). The Kuroshio Onshore Intrusion along the Shelf Break of the East China Sea: The Origin of the Tsushima Warm Current. *Journal of Physical Oceanography*, *36*, 2205-2231. <https://doi.org/10.1175/JPO2976.1>
- Guo, X., Zhu, X. H., Wu, Q. S., & Huang, D. (2012). The Kuroshio Nutrient Stream and Its Temporal Variation in the East China Sea. *Journal of Geophysical Research: Oceans*, *117*, C11006. <https://doi.org/10.1029/2011JC007292>
- Guo, Y. J. (1994). Primary Productivity and Phytoplankton in China Seas. In *Oceanology of China Seas* (pp. 227-242). Berlin: Springer. https://doi.org/10.1007/978-94-011-0862-1_24
- Hinata, T. (1996). Seasonal Variation and Long-Term Trends of the Oceanographic Conditions along a Fixed Hydrographic Line Crossing the Kuroshio in the East China Sea. *Oceanographic Magazine*, *45*, 9-32.
- Iseki, K. (1995). *Role of Continent Margins in the Global Biogeochemical Cycles: Japanese MASFLEX Program. An Interim Report of IGBP Activities in Japan, 1990-1994* (pp. 51-56).
- Isobe, A., & Matsuno, T. (2008). Long-Distance Nutrient-Transport Process in the Changjiang River Plume on the East China Sea Shelf in Summer. *Journal of Geophysical Research: Oceans*, *113*. <https://doi.org/10.1029/2007JC004248>
- Ito, T., Kaneko, A., Tsubota, H., & Gohda, N. (1994). The Characteristic Distribution of Silica over the East China Sea Shelf Slope. *Journal of Oceanography*, *50*, 465-477. <https://doi.org/10.1007/BF02234968>
- Kalnay, E., Kanamitsu, M., Kistler, R., Collins, W., Deaven, D., Gandin, L., Iredell, M., Saha, S., White, G., & Woollen, J. (1996). The NCEP/NCAR 40-Year Reanalysis Project. *Bulletin of the American Meteorological Society*, *77*, 437-472. [https://doi.org/10.1175/1520-0477\(1996\)077<0437:TNYRP>2.0.CO;2](https://doi.org/10.1175/1520-0477(1996)077<0437:TNYRP>2.0.CO;2)
- Ladd, C., Stabeno, P., & Cokelet, E. (2005). A Note on Cross-Shelf Exchange in the Northern Gulf of Alaska. *Deep Sea Research Part II: Topical Studies in Oceanography*, *52*, 667-679. <https://doi.org/10.1016/j.dsr2.2004.12.022>
- Lee, J.-S., & Takeshi, M. (2007). Intrusion of Kuroshio Water onto the Continental Shelf of the East China Sea. *Journal of Oceanography*, *63*, 309-325. <https://doi.org/10.1007/s10872-007-0030-9>
- Liang, W.-D., Tang, T., Yang, Y., Ko, M., & Chuang, W.-S. (2003). Upper-Ocean Currents around Taiwan. *Deep Sea Research Part II: Topical Studies in Oceanography*, *50*, 1085-1105. [https://doi.org/10.1016/S0967-0645\(03\)00011-0](https://doi.org/10.1016/S0967-0645(03)00011-0)
- Lie, H. J., Cho, C. H., Lee, J. H., Niiler, P., & Hu, J. H. (1998). Separation of the Kuroshio Water and Its Penetration onto the Continental Shelf West of Kyushu. *Journal of Geophysical Research: Oceans*, *103*, 2963-2976. <https://doi.org/10.1029/97JC03288>
- Liu, C., Wang, F., Chen, X., & von Storch, J. S. (2014). Interannual Variability of the Kuroshio Onshore Intrusion along the East China Sea Shelf Break: Effect of the Kuroshio Volume Transport. *Journal of Geophysical Research: Oceans*, *119*, 6190-6209. <https://doi.org/10.1002/2013JC009653>
- Liu, K.-K., Gong, G.-C., Lin, S., Yang, C.-Y., Wei, C.-L., Pai, S.-C., & Wu, C.-K. (1992). The Year-Round Upwelling at the Shelf Break near the Northern Tip of Taiwan as Evidenced by Chemical Hydrography. *Terrestrial, Atmospheric and Oceanic Sciences*, *3*, 243-275. [https://doi.org/10.3319/TAO.1992.3.3.243\(KEEP\)](https://doi.org/10.3319/TAO.1992.3.3.243(KEEP))

- Locarnini, R., Mishonov, A., Antonov, J., Boyer, T., Garcia, H., Baranova, O., Zweng, M., & Johnson, D. (2006). World Ocean Atlas 2005, Vol. 1, Temperature. In S. Levitus (Ed.), *NOAA Atlas NESDIS* (Vol. 61). Washington DC: U.S. Government Printing Office.
- Oey, L.-Y., Hsin, Y.-C., & Wu, C.-R. (2010). Why Does the Kuroshio Northeast of Taiwan Shift Shelfward in Winter? *Ocean Dynamics*, *60*, 413-426.
<https://doi.org/10.1007/s10236-009-0259-5>
- Oka, E., & Kawabe, M. (1998). Characteristics of Variations of Water Properties and Density Structure around the Kuroshio in the East China Sea. *Journal of Oceanography*, *54*, 605-617. <https://doi.org/10.1007/BF02823281>
- Qiao, F., Yang, Y., Lü, X., Xia, C., Chen, X., Wang, B., & Yuan, Y. (2006). Coastal Upwelling in the East China Sea in Winter. *Journal of Geophysical Research: Oceans*, *111*, C11S06. <https://doi.org/10.1029/2005JC003264>
- Sathyendranath, S. (2000). *Remote Sensing of Ocean Colour in Coastal, and Other Optically-Complex, Waters* (p. 3). IOCCG Report.
- Soeyanto, E., Guo, X., Ono, J., & Miyazawa, Y. (2014). Interannual Variations of Kuroshio Transport in the East China Sea and Its Relation to the Pacific Decadal Oscillation and Mesoscale Eddies. *Journal of Geophysical Research: Oceans*, *119*, 3595-3616.
<https://doi.org/10.1002/2013JC009529>
- Song, Y., & Haidvogel, D. (1994). A Semi-Implicit Ocean Circulation Model Using a Generalized Topography-Following Coordinate System. *Journal of Computational Physics*, *115*, 228-244. <https://doi.org/10.1006/jcph.1994.1189>
- Su, J., Guan, B., & Jiang, J. (1990). The Kuroshio, Part I, Physical Features. *Oceanography and Marine Biology: An Annual Review*, *28*, 11-71.
- Sugimoto, R., Kasai, A., Miyajima, T., & Fujita, K. (2009). Transport of Oceanic Nitrate from the Continental Shelf to the Coastal Basin in Relation to the Path of the Kuroshio. *Continental Shelf Research*, *29*, 1678-1688. <https://doi.org/10.1016/j.csr.2009.05.013>
- Sun, X. (1987). Analysis of the Surface Path of the Kuroshio in the East China Sea. In *Essays on Investigation of Kuroshio* (pp. 1-14). Beijing: China Ocean Press.
- Tang, T., & Yang, Y. (1993). Low Frequency Current Variability on the Shelf Break Northeast of Taiwan. *Journal of Oceanography*, *49*, 193-210.
<https://doi.org/10.1007/BF02237288>
- Tang, T., Hsueh, Y., Yang, Y., & Ma, J. (1999). Continental Slope Flow Northeast of Taiwan. *Journal of Physical Oceanography*, *29*, 1353-1362.
[https://doi.org/10.1175/1520-0485\(1999\)029<1353:CSFN0T>2.0.CO;2](https://doi.org/10.1175/1520-0485(1999)029<1353:CSFN0T>2.0.CO;2)
- Tang, T., Tai, J., & Yang, Y. (2000). The Flow Pattern North of Taiwan and the Migration of the Kuroshio. *Continental Shelf Research*, *20*, 349-371.
[https://doi.org/10.1016/S0278-4343\(99\)00076-X](https://doi.org/10.1016/S0278-4343(99)00076-X)
- Wang, B.-D., Wang, X.-L., & Zhan, R. (2003). Nutrient Conditions in the Yellow Sea and the East China Sea. *Estuarine, Coastal and Shelf Science*, *58*, 127-136.
[https://doi.org/10.1016/S0272-7714\(03\)00067-2](https://doi.org/10.1016/S0272-7714(03)00067-2)
- Wang, W., Yu, Z., Song, X., Wu, Z., Yuan, Y., Zhou, P., & Cao, X. (2016). The Effect of Kuroshio Current on Nitrate Dynamics in the Southern East China Sea Revealed by Nitrate Isotopic Composition. *Journal of Geophysical Research: Oceans*, *121*, 7073-7087. <https://doi.org/10.1002/2016JC011882>
- Wang, X., & Chao, Y. (2004). Simulated Sea Surface Salinity Variability in the Tropical Pacific. *Geophysical Research Letters*, *31*. <https://doi.org/10.1029/2003GL018146>
- Wei, H., Su, J., Wan, R. J., Wang, L., & Lin, Y. A. (2003). Tidal Front and the Conver-

- gence of Anchovy (*Engraulis japonicus*) Eggs in the Yellow Sea. *Fisheries Oceanography*, 12, 434-442. <https://doi.org/10.1046/j.1365-2419.2003.00259.x>
- Wei, Y., Huang, D., & Zhu, X.-H. (2013). Interannual to Decadal Variability of the Kuroshio Current in the East China Sea from 1955 to 2010 as Indicated by *In-Situ* Hydrographic Data. *Journal of Oceanography*, 69, 571-589. <https://doi.org/10.1007/s10872-013-0193-5>
- Whitney, F., Crawford, W., & Harrison, P. (2005). Physical Processes That Enhance Nutrient Transport and Primary Productivity in the Coastal and Open Ocean of the Subarctic NE Pacific. *Deep Sea Research Part II: Topical Studies in Oceanography*, 52, 681-706. <https://doi.org/10.1016/j.dsr2.2004.12.023>
- Wollast, R. (1991). The Coastal Organic Carbon Cycle; Fluxes, Sources, and Sinks. In R. F. C. Mantoura, J. M. Martin, & R. Wollast (Eds.), *Ocean Margin Processes in Global Change* (pp. 365-381). Chichester: Wiley.
- Wollast, R. (1993). Interactions of Carbon and Nitrogen Cycles in the Coastal Zone. In *Interactions of C, N, P and S Biogeochemical Cycles and Global Change* (pp. 195-210). Berlin: Springer. https://doi.org/10.1007/978-3-642-76064-8_7
- Wu, C. R., Hsin, Y. C., Chiang, T. L., Lin, Y. F., & Tsui, I. (2014). Seasonal and Interannual Changes of the Kuroshio Intrusion onto the East China Sea Shelf. *Journal of Geophysical Research: Oceans*, 119, 5039-5051. <https://doi.org/10.1002/2013JC009653>
- Wu, C. R., Lu, H. F., & Chao, S. Y. (2008). A Numerical Study on the Formation of Upwelling off Northeast Taiwan. *Journal of Geophysical Research: Oceans*, 113. <https://doi.org/10.1029/2007JC004697>
- Xiu, P., & Chai, F. (2014). Connections between Physical, Optical and Biogeochemical Processes in the Pacific Ocean. *Progress in Oceanography*, 122, 30-53. <https://doi.org/10.1016/j.pocean.2013.11.008>
- Yang, D. Z., Huang, R. X., Yin, B. S., Feng, X. R., Chen, H. Y., Qi, J. F., Benthuyzen, J. A. et al. (2018a). Topographic Beta Spiral and Onshore Intrusion of the Kuroshio Current. *Geophysical Research Letters*, 45, 287-296. <https://doi.org/10.1002/2017GL076614>
- Yang, D. Z., Xu, L. J., Yin, B. S., Feng, X. R., Chen, H. Y., Qi, J. F., & Cui, X. (2017). Numerical Study on Inter-Annual Variation of Cross-Shelf Intrusion of Kuroshio into In- to East China Sea. *Oceanologia et Limnologia Sinica*, 48, 1318-1327.
- Yang, D., Yin, B., Chai, F., Feng, X., Xue, H., Gao, G., & Yu, F. (2018b). The Onshore Intrusion of Kuroshio Subsurface Water from February to July and a Mechanism for the Intrusion Variation. *Progress in Oceanography*, 167, 97-115. <https://doi.org/10.1016/j.pocean.2018.08.004>
- Yang, D., Yin, B., Liu, Z. et al. (2012). Numerical Study on the Pattern and Origins of Kuroshio Branches in the Bottom Water of Southern East China Sea in Summer. *Journal of Geophysical Research Oceans*, 117, C02014. <https://doi.org/10.1029/2011JC007528>
- Yang, D., Yin, B., Liu, Z., & Feng, X. (2011). Numerical Study of the Ocean Circulation on the East China Sea Shelf and a Kuroshio Bottom Branch Northeast of Taiwan in Summer. *Journal of Geophysical Research: Oceans*, 116, C05015. <https://doi.org/10.1029/2010JC006777>
- Yang, D., Yin, B., Sun, J., & Zhang, Y. (2013). Numerical Study on the Origins and the Forcing Mechanism of the Phosphate in Upwelling Areas off the Coast of Zhejiang Province, China in Summer. *Journal of Marine Systems*, 123, 1-18. <https://doi.org/10.1016/j.jmarsys.2013.04.002>
- Zhang, J., Liu, S., Ren, J., Wu, Y., & Zhang, G. (2007). Nutrient Gradients from the Eutrophic Changjiang (Yangtze River) Estuary to the Oligotrophic Kuroshio Waters and

Re-Evaluation of Budgets for the East China Sea Shelf. *Progress in Oceanography*, 74, 449-478. <https://doi.org/10.1016/j.pocean.2007.04.019>

Zhang, S., Zhang, C., Wang, L., Zhang, L., Chen, X., & Wang, M. (1997). *Contents of Rare Elements and Mass Transport Rate of C, N, P, S in the Changjiang River, Sources, Transport and Environmental Impact of Contaminants in the Coastal and Estuarine Areas of China* (pp. 5-18).

Zhao, L., & Guo, X. (2011). Influence of Cross-Shelf Water Transport on Nutrients and Phytoplankton in the East China Sea: A Model Study. *Ocean Science*, 7, 27-43. <https://doi.org/10.5194/osd-7-1405-2010>

Zhu, X.-H., Park, J.-H., & Kaneko, I. (2006). Velocity Structures and Transports of the Kuroshio and the Ryukyu Current during Fall of 2000 Estimated by an Inverse Technique. *Journal of oceanography*, 62, 587-596. <https://doi.org/10.1007/s10872-006-0078-y>